Energy dependence of the (*e*,2*e*) recoil peak to binary peak ratio across He $(2p^2)^1D$ and $(2s2p)^1P$ autoionizing levels

B. A. deHarak,[1] K. Bartschat,[2] and N. L. S. Martin[3,*]

[1]*Physics Department, Illinois Wesleyan University, P.O. Box 2900, Bloomington, Illinois 61702-2900, USA*
[2]*Department of Physics and Astronomy, Drake University, Des Moines, Iowa 50311, USA*
[3]*Department of Physics and Astronomy, University of Kentucky, Lexington, Kentucky 40506-0055, USA*

The (*e*,2*e*) recoil peak to binary peak ratio as a function of the ejected-electron energy is reported for helium autoionizing levels $(2p^2)^1D$ and $(2s2p)^1P$. A special out-of-plane geometry is used where the ejected electrons are detected in a plane that includes the momentum transfer axis but is perpendicular to the scattering plane. The measured recoil peak to binary peak ratio is a dimensionless quantity that can be directly compared with calculations. A second-order model in the projectile-target interaction correctly reproduces the observed energy dependence and magnitude of the ratio, while a first-order model does not.

PACS number(s): 34.80.Dp

I. INTRODUCTION

A typical electron-electron coincidence, or (*e*,2*e*), experiment investigates the angular distribution of ejected electrons, of momentum $\boldsymbol{k}_{ej}$, measured in coincidence with scattered electrons of momentum $\boldsymbol{k}_{sc}$, following electron-impact ionization of an atomic target by an incident beam of linear momentum $\boldsymbol{k}_0$. Such angular distributions of ejected electrons show two pronounced features, the binary and recoil peaks, which are aligned approximately parallel and antiparallel to the momentum transfer $\boldsymbol{K} = \boldsymbol{k}_0 - \boldsymbol{k}_{sc}$. The binary peak is named after the binary-encounter approximation [1,2], in which the atomic electrons are considered to be free, resulting in billiard-ball-type collisions where the ejected electron carries away all the momentum transferred to the target [1]. The origin of the recoil peak has been qualitatively explained by Vriens [1] as being due to reflection of the outgoing ionized electron, initially in the momentum-transfer direction, by the atomic potential field, in the same way that a positive-energy electron can be reflected by a simple square well or barrier potential. The size of these peaks depends on both the target and the kinematics of the reaction.

For direct ionization, the relative size of the recoil and binary peaks provides important clues about the collision dynamics, especially regarding the potential influence of resonances and high-order effects. It can also serve as a benchmark for testing state-of-the-art theoretical approaches. Thus experimental and theoretical studies of He, Ne, and Ar [3,4], carried out for a fixed scattering angle $\theta_{sc} = 6°$ and scattered-electron energy of 500 eV, found recoil to binary ratios ($\mathcal{R}_{RB}$) that were pronounced functions of ejected-electron energy. For He, the recoil peak was generally much smaller than the binary peak, and $\mathcal{R}_{RB}$ was <0.2 for ejected-electron energies >20 eV. The He results were in qualitative agreement with Vriens' model: the larger the momentum transfer, the smaller the value of $\mathcal{R}_{RB}$. This, however, was not the case for the other targets; for Ne and Ar the recoil peak became larger than the binary peak as the ejected-electron energy was increased, with $\mathcal{R}_{RB} \approx 2$ at 300 eV. This was explained in terms of the phase shifts

of the ejected electron partial waves, and an anomalously large recoil peak intensity in Ne $2s^2$ was reproduced satisfactorily by partial-wave reflection from a short-range Hartree-Fock potential [4].

For direct ionization $\mathcal{R}_{RB}$ is a slowly varying function of the ejected-electron energy. This is not expected to be the case for autoionizing states, where all quantities vary rapidly over the resonance width [5]. In previous work we measured (*e*,2*e*) ejected-electron angular distributions for the He autoionizing levels $(2s^2)^1S$, $(2p^2)^1D$, and $(2s2p)^1P$, and also for direct ionization, with an incident electron energy of 488 eV and scattering angle of 20.5°[6,7]. We used a special out-of-plane geometry, which included the momentum transfer axis but was perpendicular to the scattering plane. Because of reflection symmetry in the scattering plane, the observed binary and recoil peaks were in the $\pm\hat{\boldsymbol{K}}$ directions [8].

The recoil peak for direct ionization was negligible (in agreement with Vriens' model for large momentum transfer), whereas the three autoionizing levels had pronounced recoil peaks. We explained the recoil peaks as being due to the resonant behavior of the $\ell = L$ partial wave, where L is the orbital angular momentum of a particular resonance. A simple plane-wave Born calculation in the Balashov *et al.* formalism [9], which included a resonant partial wave, was able to reproduce the experimental results, albeit with very large fitted Fano q parameters. We also carried out sophisticated first-order and second-order hybrid distorted wave + convergent R matrix with pseudostates (close-coupling) calculations (DWB1-RMPS and DWB2-RMPS, respectively). It was found that the first-order calculations severely underestimated the recoil peak but the second-order calculations were in excellent agreement with the experiments.

These experimental angular distributions were energy integrated over the width of each resonance. We have now carried out more detailed experiments that investigate the energy dependence of $\mathcal{R}_{RB}$, for our out-of-plane geometry and the same kinematics, over the He $(2p^2)^1D$ and $(2s2p)^1P$ resonances. Below we present the results of these experiments, in comparison with our first-order and second-order calculations.

———
*nmartin@uky.edu

II. THEORY

Details of the DWB1-RMPS and DWB2-RMPS methods are given elsewhere [10–13]. The essential point is that the (fast) projectile–target interaction is treated perturbatively to first (DWB1) or second (DWB2) order, while the initial bound state and the e-He$^+$ half-collision of a slow ejected electron and the residual ion are treated via a convergent close-coupling expansion. The two types of calculations yield very different results, particularly for the intensity of the recoil peak. The difference can be traced to real and complex effective Fano q parameters [5] for the first and second-order calculations, respectively [14].

Our calculations show that the maximum of the binary peak along $+\hat{\boldsymbol{K}}$, although it can become small, never vanishes exactly, and the recoil peak to binary peak ratio, given by the intensities along $-\hat{\boldsymbol{K}}$ and $+\hat{\boldsymbol{K}}$, remains finite in both the first-order and the second-order models, with a maximum value of about 40 for the latter. The calculations predict an energy dependence of this ratio with very sharp resonant behavior for the two resonances, with widths much narrower than our experimental energy resolution of about 100 meV.

Our previous experiments [6] show that the binary peak occupies the angular range $\phi = 0 \to 30°$, and the recoil peak occupies the range $\phi = 150° \to 180°$, where $\phi = 0, 180°$ corresponds to $+\hat{\boldsymbol{K}}, -\hat{\boldsymbol{K}}$, respectively. The rapid variation in $\mathcal{R}_{RB}$ is much reduced if we sum over these angles. For the purposes of this paper we have therefore defined a recoil to binary peak ratio in terms of the sums over selected ejected-electron directions used in our experiments as

$$\mathcal{R}_{RB} = \frac{I_{180} + I_{165} + I_{150}}{I_0 + I_{15} + I_{30}}, \quad (1)$$

where I_ϕ is the $(e,2e)$ intensity for a particular ejected-electron direction. (Note that this definition of $\mathcal{R}_{RB}$ is not a parametrization of the whole angular distribution since it does not include the out-of-plane region $\phi = 30° \to 150°$.) Figure 1 shows the calculated behavior of $\mathcal{R}_{RB}$ over the energy range and kinematics of our experiments. For the second-order calculations, the calculated maximum values of $\mathcal{R}_{RB}$ for the $(2p^2)^1D$ and $(2s2p)^1P$ resonances are then about 9 and 7, respectively, with corresponding widths of approximately 30
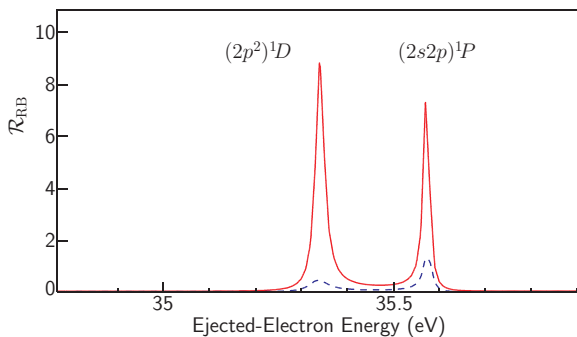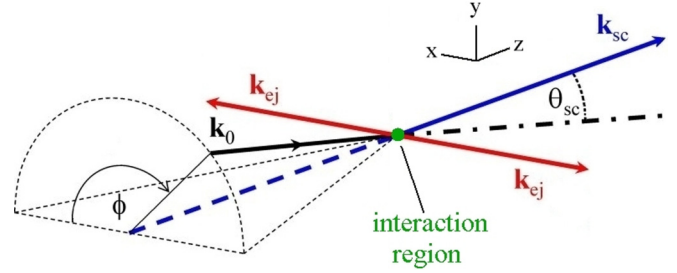
FIG. 2. (Color online) Geometry of the apparatus. The incident ($\boldsymbol{k}_0$) and the detected ejected ($\boldsymbol{k}_{ej}$) and scattered ($\boldsymbol{k}_{sc}$) electron directions are indicated.

and 20 meV. These are about a factor of 2 less than the calculated spectral widths of 64 and 38 meV [14]. For the first-order calculations, the calculated maximum values of $\mathcal{R}_{RB}$ are almost an order of magnitude smaller.

III. EXPERIMENTAL METHOD

The experimental apparatus is described in detail elsewhere [8,15]. It consists of an unmonochromated electron gun, a gaseous target beam, two ejected-electron spectrometers, and a scattered-electron spectrometer. The two ejected-electron spectrometers are at angles $\pm 90°$ with respect to the scattered-electron spectrometer. The gun can move on the surface of a cone of half-angle θ_{sc} whose axis lies in the scattered-electron detector direction. This is illustrated in Fig. 2, which shows the trajectories of the incident, scattered, and ejected electrons. This geometry is equivalent to rotating the ejected-electron detectors around z while keeping the gun and scattered-electron detector fixed. Thus, as the gun position is varied from $\phi = 0 \to 180°$, the ejected detector on the left effectively varies from $\phi_{ej} = 0$ to $\phi_{ej} = -180°$, and the ejected detector on the right effectively varies from $\phi_{ej} = 180°$ to $\phi = 0$, with a combined range equal to the full $\phi_{ej} = 0 \to 360°$.

This configuration enables us to carry out a special type of out-of-plane measurement where the momentum transfer vector is perpendicular to the scattered-electron direction. For an incident electron of energy E_0, the condition for this is $\theta_{sc} = \arcsin\left(\sqrt{\Delta E/E_0}\right)$, where ΔE is the energy loss; i.e., the energy of the $2\ell 2\ell'$ autoionizing levels above the ground state ≈ 60 eV. The corresponding momentum transfer is $K = \sqrt{2\Delta E}$, which is independent of the initial energy and has the value $K = 2.1$ a.u. in the autoionizing region.

The experiments reported here were carried out with an incident electron energy $E_0 = 488$ eV, for which the desired scattering angle is $\theta_{sc} = 20.5°$. With these kinematics the measured $(e,2e)$ out-of-plane angular distribution of ejected electrons corresponds to a plane containing the momentum transfer vector $\boldsymbol{K}$; it is perpendicular to $\boldsymbol{k}_{sc}$ and hence also to the scattering plane. In this sense we do not measure the true maxima of the binary and recoil peaks, but at the high incident electron beam energy of the experiments, these are expected to lie close to the momentum transfer axis.

The effective geometry of the experiments is represented in Fig. 3, where plane I (the xz plane) is the scattering plane containing the incident-electron, scattered-electron, and momentum transfer directions. Plane II (the yz plane) is

FIG. 1. (Color online) Calculated $(e,2e)$ angular distribution recoil peak to binary peak ratio, $\mathcal{R}_{RB}$ [Eq. (1)], over the helium $(2p^2)^1D$ and $(2s2p)^1P$ autoionizing resonances, for 488-eV electrons scattered through $20.5°$. Solid (red) and dashed (blue) lines represent DWB2-RMPS and DWB1-RMPS calculations, respectively.
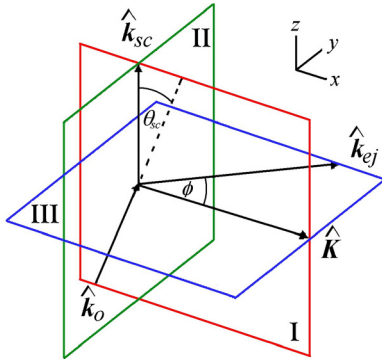
FIG. 3. (Color online) Effective geometry of the present experiments. Plane I is the scattering plane containing the incident-electron ($\hat{\boldsymbol{k}}_0$), scattered-electron ($\hat{\boldsymbol{k}}_{sc}$), and momentum transfer ($\hat{\boldsymbol{K}}$) directions. Plane II is the plane perpendicular to both the scattering plane and the momentum transfer direction. Our experiments measure the (*e*,2*e*) angular distribution of ejected electrons ($\hat{\boldsymbol{k}}_{ej}$) as a function of ϕ in plane III. See text for details.

the plane perpendicular to both the scattering plane and the momentum transfer direction. Our experiments measure the (*e*,2*e*) ejected-electron angular distribution as a function of ϕ in plane III (the xy plane), which contains the momentum transfer direction but is perpendicular to the scattering plane.

Data were taken from $\phi = 0$ to $\phi = 180°$ in 15° intervals for one ejected-electron detector, which corresponds to $\phi = 180° \rightarrow 360°$ for the other detector. Because there is reflection symmetry in the scattering plane, the results for $\phi = 360° \rightarrow 180°$ could be added to those for $\phi = 0 \rightarrow 180°$ to improve statistics and also to minimize any apparatus effects. At each angle an (*e*,2*e*) spectrum was collected in 30-meV steps over a range of 2 eV that included the He $(2p^2)^1D$ and $(2s2p)^1P$ resonances. The energy resolution was determined by fitting the two line shapes in the simultaneously measured high-quality noncoincidence spectra; for the present experiments the instrument function was taken to be a Gaussian and had a full width at half-maximum (FWHM) of about 100 meV. The fits were also used to calibrate the energy scale from the known values of the resonance positions [16]. Note that to compare theory and experiment, $\mathcal{R}_{RB}$ is formed from the calculated
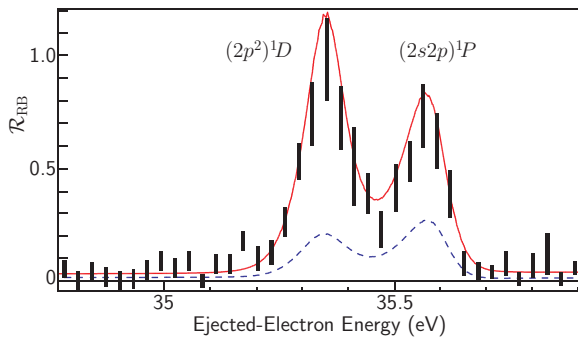
FIG. 4. (Color online) Observed (*e*,2*e*) angular distribution recoil peak to binary peak ratio, $\mathcal{R}_{RB}$ [Eq. (1)], over the helium $(2p^2)^1D$ and $(2s2p)^1P$ autoionizing resonances, for 488-eV electrons scattered through 20.5°. Vertical bars represent the experimental results and indicate the statistical errors. Solid (red) and dashed (blue) lines are DWB2-RMPS and DWB1-RMPS calculations, respectively.
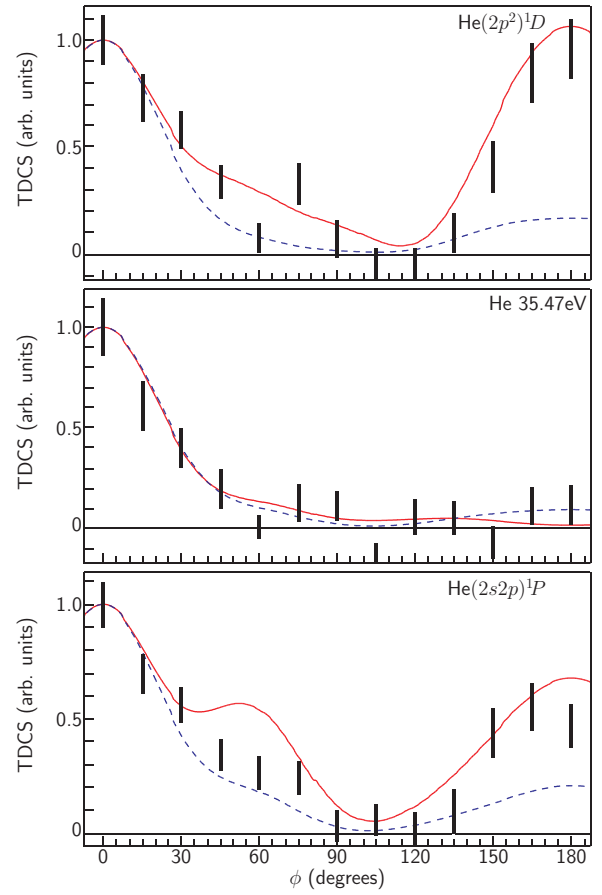
FIG. 5. (Color online) Helium out-of-plane (*e*,2*e*) ejected-electron angular distributions for the $(2p^2)^1D$ and $(2s2p)^1P$ resonances, and the minimum that lies between them at 35.47 eV in Fig. 4. Vertical bars represent the experimental results and indicate statistical errors. Solid (red) and dashed (blue) lines are DWB2-RMPS and DWB1-RMPS calculations, respectively. Theory and experiment are normalized to unity at $\phi = 0$.

recoil and binary peak spectra after they are separately convoluted with the experimental Gaussian instrument function. No corrections were deemed necessary for the angular acceptances of the detectors: that of the scattered-electron detector was $\sim \pm 1°$ (small compared with the 20.5° scattering angle), and that of the ejected-electron detector was $\sim \pm 5°$ (over which the angular distribution varies very little).

The data were corrected as described in Ref. [8], except that the scattered-electron detector correction was omitted; it was found that a small variation in scattering angle about the correct value led to only small changes in the measured (*e*,2*e*) angular distributions but led to a relatively large change in the scattered-electron detector correction factor.

IV. RESULTS AND DISCUSSION

The experimental results and theoretical predictions are shown in Figs. 4 and 5. Figure 4 shows the (*e*,2*e*) angular distribution recoil peak to binary peak ratio, $\mathcal{R}_{RB}$, defined by Eq. (1), over the energy range of the helium $(2p^2)^1D$ and $(2s2p)^1P$ autoionizing resonances. Note that because $\mathcal{R}_{RB}$ is a dimensionless ratio, there is a direct comparison

of experiment and theory. Everywhere except in the resonance region, $\mathcal{R}_{\mathrm{RB}}$ is very small, somewhat less than 0.1. In the region of the two resonances $\mathcal{R}_{\mathrm{RB}}$ changes rapidly: even with our energy resolution of 100 meV, $\mathcal{R}_{\mathrm{RB}}$ reaches values close to unity; i.e., the recoil peak is as important as the binary peak. The DWB2-RMPS results are in good agreement with the experimental data, but the DWB1-RMPS calculations seriously underestimate the resonant values of $\mathcal{R}_{\mathrm{RB}}$, and in fact the first-order model incorrectly predicts that $\mathcal{R}_{\mathrm{RB}}$ for the $(2s2p)^1P$ resonance is larger than that for the $(2p^2)^1D$ resonance.

Finally, Fig. 5 shows the full $(e,2e)$ angular distributions for the $(2p^2)^1D$ and $(2s2p)^1P$ resonances and the minimum that lies between them. For each resonance, the angular distributions were summed over the three energies corresponding to the maximum values of $\mathcal{R}_{\mathrm{RB}}$ (see Fig. 4); for the minimum, the angular distribution was that measured at 35.47 eV. The second-order calculation for the $(2p^2)^1D$ resonance is in good agreement with the experimental angular distribution, to within the statistics, over the entire angular range. On the other hand, the second-order calculation for the $(2s2p)^1P$ resonance is in good agreement with the experiment in the recoil peak but is in poor agreement in the out-of-plane region around $\phi = 50°$.

V. SUMMARY AND CONCLUSIONS

We have measured the recoil peak to binary peak ratio $\mathcal{R}_{\mathrm{RB}}$ over the He $(2p^2)^1D$ and $(2s2p)^1P$ autoionizing resonances.

We find a very strong dependence on the ejected-electron energy, with maximum values approaching unity, even with an energy resolution of 100 meV. There is good agreement with second-order calculations but poor agreement with first-order calculations. In our earlier work [6,7], which integrated over each resonance, the averaged value of $\mathcal{R}_{\mathrm{RB}}$ was about 0.3 for both resonances; clearly the present experiments are a worthwhile probe of the detailed energy dependence predicted in the calculations and confirm the disagreement of the out-of-plane region for the $(2s2p)^1P$ resonance; a direct comparison with our earlier angular distributions can be made by comparing Fig. 5 here with Fig. 3 in Ref. [7].

Finally, we note that whereas for the case of Ne the anomalously large recoil peak was ascribed to the phase shifts of all partial waves in a Hartree-Fock potential [3,4], for He autoionization the large recoil peaks can be ascribed to an enhanced amplitude for a single partial wave for each resonance, specifically the d wave for $(2p^2)^1D$ and the p wave for $(2s2p)^1P$.

[1] T. Vriens, Physica **45**, 400 (1969).

[2] H. Ehrhardt, M. Schulz, T. Tekaat, and K. Willmann, Phys. Rev. Lett. **22**, 89 (1969).

[3] A. S. Kheifets, A. Naja, E. M. S. Casagrande, and A. Lahmam-Bennani, J. Phys. B **41**, 145201 (2008).

[4] A. S. Kheifets, A. Naja, E. M. S. Casagrande, and A. Lahmam-Bennani, J. Phys. B **42**, 165204 (2009).

[5] U. Fano, Phys. Rev. **124**, 1866 (1961).

[6] B. A. deHarak, K. Bartschat, and N. L. S. Martin, Phys. Rev. Lett. **100**, 063201 (2008).

[7] B. A. deHarak, K. Bartschat, and N. L. S. Martin, Phys. Rev. A **82**, 062705 (2010).

[8] B. A. deHarak and N. L. S. Martin, Meas. Sci. Technol. **19**, 015604 (2008).

[9] V. V. Balashov, S. S. Lipovetskiǐ, and V. S. Senashenko, Sov. Phys. JETP **36**, 858 (1973).

[10] K. Bartschat and P. G. Burke, J. Phys. B **20**, 3191 (1987).

[11] R. H. G. Reid, K. Bartschat, and A. Raeker, J. Phys. B **31**, 563 (1998); **33**, 5261 (2000).

[12] Y. Fang and K. Bartschat, J. Phys. B **34**, L19 (2001).

[13] K. Bartschat and A. N. Grum-Grzhimailo, J. Phys. B **35**, 5035 (2002).

[14] N. L. S. Martin, B. A. deHarak, and K. Bartschat, J. Phys. B **42**, 225201 (2009).

[15] B. A. deHarak, J. G. Childers, and N. L. S. Martin, J. Electr. Spectr. Rel. Phen. **141**, 75 (2004).

[16] B. A. deHarak, J. G. Childers, and N. L. S. Martin, Phys. Rev. A **74**, 032714 (2006).